

# Temperature Effect on a Lumped Element Balanced Dual-Band Band-Stop Filter

Dubari Borah and Thottam S. Kalkur\*

**Abstract**—In this manuscript, the thermal effect on a lumped element balanced (differential) dual-band band-stop filter (BSF) has been discussed in detail for the first time. The response of a novel filter should maintain consistency over a wide range of temperature. Although any microwave filter in general is designed for room temperature condition, the filter is employed for applications where the operating temperature constantly changes. Therefore, it is necessary to check the reliability of the filter response within a specific temperature range based on its application. Modern simulation software helps to make an initial assumption about the filter performance at different thermal conditions before its lab testing or actual application. Here, a quantitative analysis has been provided to show how change in temperature contributes to the change in each component value of a lumped element filter. This analysis is followed by a simulation to show that a balanced lumped element filter exhibits lower loss than its single-ended counterpart. Also, as the temperature varies, the balanced design demonstrates less deviation in the loss value than a two-port design. Next, a balanced dual-band BSF prototype with center frequencies 1.151 GHz and 1.366 GHz (25°C) is characterized with a 4-port network analyzer under different temperature conditions. The experimental results exhibit a good match with the simulation results. For a variation of 80°C in temperature, the maximum deviation obtained for the filter center frequency, absolute bandwidth (ABW), and insertion loss (Sdd21) are 5 MHz, 2.8 MHz and 2 dB, respectively.

## 1. INTRODUCTION

With the evolution of multiband wireless standards such as LTE networks, the demand of multiband filter is growing rapidly [1–4]. A decade ago, if a smartphone was able to handle only five frequency bands, it was declared as world phone, but with the proliferation of LTE technology, this requirement is increased to a minimum of 50 bands. Each of these frequency bands requires two or more filter dies which makes a necessity of more than 100 filters in a single smartphone module. Some of these filters are designed to produce band stop response as they play an important role by protecting the required signals from outside interference or jamming [5]. To achieve better noise immunity, the balanced structures of these filters are preferred to their single-ended counterparts [6–9]. Some of the novel multiband balanced band stop filter (BSF) structures with different features have been discussed in [1, 10–13].

Generally, microwave filters are designed for room temperature, but in real world, they are required to operate under different temperature conditions. For example, the filters used for automotive applications should be functional over a wide range of temperature from  $-40^{\circ}\text{C}$  to  $125^{\circ}\text{C}$  whereas these temperature ranges for military and industrial appliances are  $(-55^{\circ}\text{C})-(+125^{\circ}\text{C})$  and  $(-20^{\circ}\text{C})-(85^{\circ}\text{C})$ , respectively. This variation in operating temperature might affect the filter response in different ways. That is why, it is important to study the temperature effect on filter response once the satisfactory

---

*Received 29 June 2020, Accepted 29 September 2020, Scheduled 12 October 2020*

\* Corresponding author: Thottam S. Kalkur (tkalkur@uccs.edu).

The authors are with the Microelectronics Research Laboratory, Department of Electrical and Computer Engineering, University of Colorado, Colorado Springs, CO 80918-7150, USA.

results are obtained at room temperature. In [14] and [15], two bandpass filter structures are considered to examine the temperature effect on their frequency responses. The vias used in these two-port designs create noise, and this noise varies with the operating temperature. It causes both the insertion loss and return loss of the filter to fluctuate with temperature. Another disadvantage of the design in [14] is that its center frequency shifts significantly with the change of operating temperature, and it needs an external temperature compensation system to stabilize it. On the other hand, only simulation results are available in [15] to show temperature effect on filter response whereas the design is not practically validated to support the simulation. The simulation results demonstrate that the resonant frequency shifts about 0.6% for only 49°C variation in operating temperature. Similarly, in [16–20], the impact of temperature is examined on various band-stop filter architectures. Among them, the designs in [16–18] have been tested for a temperature variation range of less than 40°C, and in this range, they exhibited at least 0.9% shift in their corresponding resonant frequencies. In [17], a master-slave filter circuit has been discussed to alleviate the impact of temperature on resonant frequency. Moreover, the stopband rejection in [16] is not satisfactory (maximum 10 dB). Likewise, the temperature change in [19] and [20] affects the filter designs significantly in terms of stopband resonant frequency and stopband rejection, respectively. In comparison to these single-ended designs, differential filters are highly stable in terms of system noise, generation of transient noise, voltage swing, second-order nonlinearities, and speed. That is why the use of balanced topology is not only limited to microwave filter design but also widely used in designing many other RF and microwave devices including amplifiers, oscillators, mixers, antennas, etc. The absence of vias in a balanced filter greatly reduces the temperature dependence of its frequency response, making it useful for a wide range of temperature conditions. However, to the best of the authors' knowledge, there is no literature available which examines the performance of a balanced filter structure at varying temperature.

This paper conducts a study on the functionality of a lumped element differential dual-band BSF under changing operating temperature. Due to its inherent balanced property, it exhibits almost a stable filter response over a broad temperature range, without using any additional circuitry to offset the thermal effect. The discussion here starts with a quantitative analysis of the temperature effect on each lumped component, and considering these effects, the filter is simulated in the next step. The simulated results show a good match with the experimental results.

The paper is organized as follows. Section 2 provides a theoretical foundation on how changing temperature affects the ideal lumped components. Then this study is extended to consider parasitic resistance associated with the real inductor and capacitor models. Also, this differential model is compared to its equivalent single-ended design in terms of their frequency responses within the same temperature variation range. In Section 3, the results from the simulation are compared to the experimental ones to show a good match between them. Finally, the main points of this research are summarized as the conclusion in Section 4.

## 2. THEORETICAL FOUNDATION

The balanced dual band design considered here is taken from [13] with  $f_1 = 1.151$  GHz,  $f_2 = 1.366$  GHz, and  $\Delta_1 = \Delta_2 = 6\%$ . Each lumped element used in this design is sensitive to applied temperature which affects the overall filter response. Let us start with resistor. If a conductor has a temperature coefficient of resistance (or resistivity)  $\alpha$ , the conductor resistance  $R(T_0)$  at reference temperature  $T_0$  (usually room temperature) will change at temperature  $T$ , and the resistance value at  $T$  is given by

$$R(T) = R(T_0)[1 + \alpha(T - T_0)] \quad (1)$$

Similarly, the dielectric constant of any capacitor or any PCB substrate is expressed as a function of temperature as follows [15]

$$\varepsilon_r(T) = \varepsilon_r(T_0) \left[ 1 + \beta_1(T - T_0) + \beta_2(T - T_0)^2 \right] \quad (2)$$

where  $\varepsilon_r(T)$  is the relative dielectric constant at any temperature  $T$ ;  $\varepsilon_r(T_0)$  is the relative dielectric constant at ambient temperature  $T_0$ ;  $\beta_1$  and  $\beta_2$  are the coefficients of first order and second order thermal expansions, respectively.  $\beta_2$  value is almost negligible for class 1 capacitors. Moreover, real capacitor has an equivalent series resistance (ESR) which is a combination of ohmic resistance of the

conductive part and the dielectric resistance. At high frequencies, the ohmic part of the ESR dominates, and as the temperature increases, it reduces the Q-factor associated with the capacitor.

Moreover, as the temperature varies, the geometry of any wire wound inductor changes due to thermal expansion or contraction. As the inductance of a coil is directly proportional to its area and inversely proportional to its length, the overall variation in the inductance value is also proportional to the coefficient of thermal expansion (CTE) of the coil material, as shown in Eq. (3). Besides this, the coil material retains an  $\alpha$  value for which the resistance associated with the coil also changes with temperature, resulting in a change of inductor Q-factor.

$$L(T) = L(T_0)[1 + (CTE)(T - T_0)] \tag{3}$$

Here,  $L(T_0)$  and  $L(T)$  are the inductances at reference temperature  $T_0$  (where CTE is specified) and conductor temperature  $T$ , respectively.

### 2.1. Ideal Circuit Simulation

First, an ideal circuit simulation is performed without considering the parasitic resistance effect of inductors and capacitors. Figure 1(a) shows the circuit using ideal high-Q components where each resonant frequency of the dual band frequency response is calculated as follows where  $\omega_{pi} = 2\pi f_i$  and

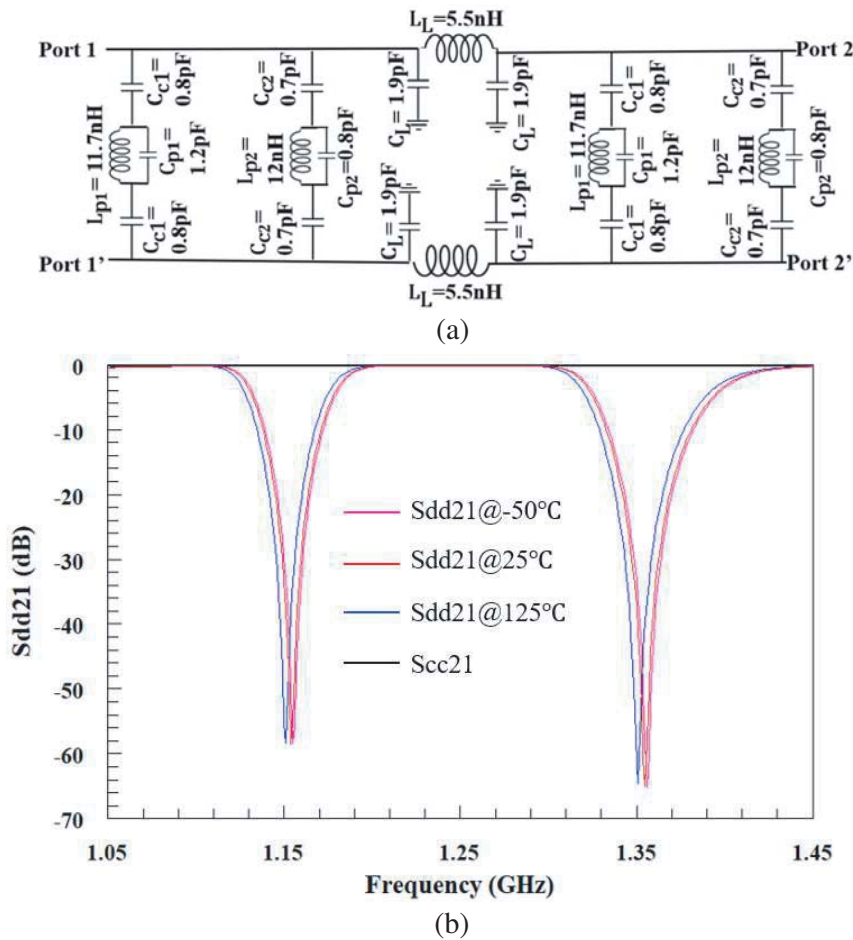


**Figure 1.** (a) Differential dual-band lumped element BSF [13] and (b) its simulation results at different temperatures where Sdd21 and Scc21 are differential insertion loss and common mode insertion loss, respectively.

$i = 1, 2$  for lower band and upper band, respectively [12, 13].

$$\omega_{pi} = \frac{1}{\sqrt{L_{pi}(C_{pi} + C_{ci})}} \quad (4)$$

Figure 1(b) shows the simulation results by varying the temperature from  $-50^\circ\text{C}$  to  $125^\circ\text{C}$ . Here, the linear temperature coefficients for capacitor and inductor are considered as  $+30 \text{ ppm}/^\circ\text{C}$  and  $+14.2 \text{ ppm}/^\circ\text{C}$ , respectively. For these positive coefficients, it is seen that the resonant frequency of each differential band slightly shifts towards right as the temperature decreases. It is obvious because the values of  $L_{P1}$ ,  $L_{P2}$ ,  $C_{P1}$ , and  $C_{P2}$  decrease with decrease in temperature, and resonant frequency is inversely proportional to these. As a result, both resonant frequencies shift towards higher values. However, the differential insertion loss (Sdd21) for each stopband remains almost constant for this entire temperature range because of the constant Q-components. Table 1 shows that for this  $175^\circ\text{C}$  variation range, the resonant frequency of each band is shifted by about 5 MHz whereas the ABW remains constant.

**Table 1.** Deviation in center frequency and absolute bandwidth of the filter response with temperature variation.

Temp ( $^\circ\text{C}$ )	$L_{p1}, L_{p2}$ (nH)	$C_{p1}, C_{p2}$ (pF)	$C_{c1}, C_{c2}$ (pF)	$f_1, f_2$ (GHz)	ABW <sub>1</sub> , ABW <sub>2</sub> (MHz)
-50	11.69, 11.99	1.2, 0.8	0.8, 0.7	1.151, 1.351	70 MHz, 81 MHz
25	11.7, 12	1.2, 0.8	0.8, 0.7	1.154, 1.355	70 MHz, 81 MHz
125	11.72, 12.02	1.2, 0.8	0.8, 0.7	1.155, 1.356	70 MHz, 81 MHz

## 2.2. Simulation Using Real Components

In [12] and [13], 0402 series wirewound inductors and 0805 series ceramic capacitors from Johanson Technology have been used on a Rogers R04003C board for the fabrication of the dual-band balanced BSF prototype. The thermal coefficient  $\beta_1$  of these ceramic capacitors varies between  $+/- 30 \text{ ppm}/^\circ\text{C}$  whereas the gold used for the wire wound inductors has a CTE value of  $+14.2 \text{ ppm}/^\circ\text{C}$ . Besides these, Rogers R04003C substrate has a relative dielectric constant ( $\epsilon_r$ ) of 3.38 at  $25^\circ\text{C}$ . This value changes from 3.37 at  $-50^\circ\text{C}$  to 3.39 at  $125^\circ\text{C}$ . In Table 2, the component values and their associated parameters at  $25^\circ\text{C}$  are taken from the datasheets, and their values at various temperatures are calculated using Equations (1)–(3). Here,  $R_{Lp1}$ ,  $R_{Lp2}$ , and  $R_{LL}$  are series resistances associated with  $L_{p1}$ ,  $L_{p2}$ , and  $L_L$ , respectively. Similarly,  $Q_{Cp1}$ ,  $Q_{Cp2}$ ,  $Q_{CL}$ ,  $Q_{Cc1}$ , and  $Q_{Cc2}$  are Q-factors of  $C_{p1}$ ,  $C_{p2}$ ,  $C_L$ ,  $C_{c1}$ , and  $C_{c2}$ , respectively.

Considering these real components, the simulation results of Figure 1(a) are demonstrated in Figure 2 and Figure 3 for  $\beta_1 = +30 \text{ ppm}/^\circ\text{C}$  and  $\beta_1 = -30 \text{ ppm}/^\circ\text{C}$ , respectively. For  $\beta_1 = +30 \text{ ppm}/^\circ\text{C}$ ,

**Table 2.** Calculation of different components and their associated parameters at various temperatures.

Temperature ( $^\circ\text{C}$ )	$L_{p1}, L_{p2}$ (nH)	$C_{p1}, C_{p2}, C_L$ (pF)	$C_{c1}, C_{c2}$ (pF)	$R_{Lp1}, R_{Lp2}, R_{LL}$ (m $\Omega$ )	$Q_{Cp1}, Q_{Cp2}, Q_{CL}$	$Q_{Cc1}, Q_{Cc2}$
25	11, 12	1.2, 0.8	0.8, 0.7	8, 8, 5	1014, 1304, 882	1304, 1558
125 with $\beta_1 = 30 \text{ ppm}/^\circ\text{C}$	11.02, 12.02	1.2, 0.8	0.8, 0.7	10, 10, 7	1011, 1301, 879.7	1301, 1553
(-50) with $\beta_1 = 30 \text{ ppm}/^\circ\text{C}$	10.99, 11.99	1.2, 0.8	0.8, 0.7	6, 6, 4	1017, 1307, 884.5	1307, 1562
125 with $\beta_1 = -30 \text{ ppm}/^\circ\text{C}$	11.02, 12.02	1.2, 0.8	0.8, 0.7	5, 5, 3	1018, 1309, 886	1309, 1564
(-50) with $\beta_1 = -30 \text{ ppm}/^\circ\text{C}$	10.99, 11.99	1.2, 0.8	0.8, 0.7	10, 10, 6	1012, 1301, 880	1301, 1554

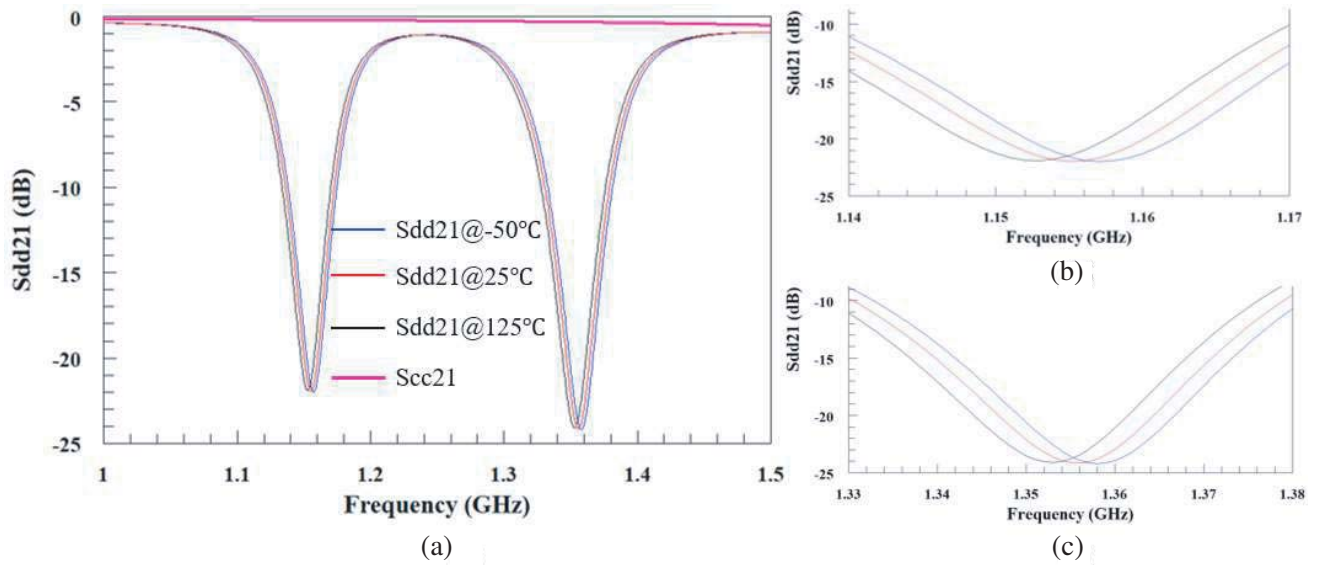


**Figure 2.** Simulation using real components where  $\beta_1$  is +30 ppm/°C. (a) Sdd21 and Scc21 plots, (b) zoomed view of lower band Sdd21 and (c) zoomed view of upper band Sdd21.

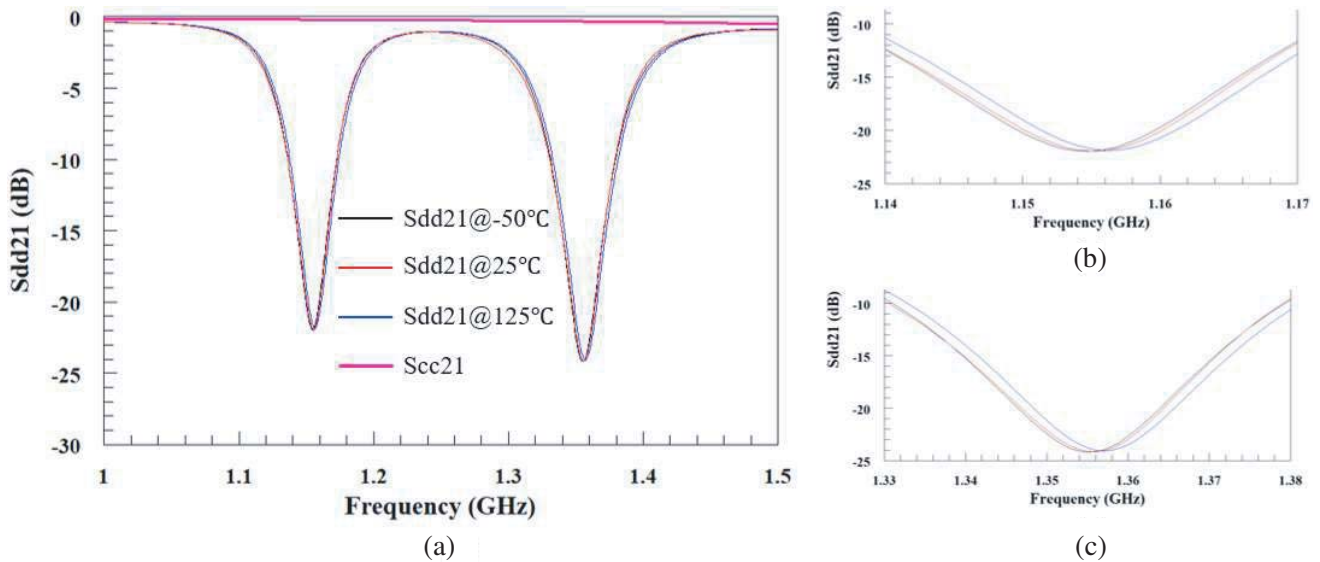


**Figure 3.** Simulation using real components where  $\beta_1$  is -30 ppm/°C. (a) Sdd21 and Scc21 plots, (b) zoomed view of lower band Sdd21 and (c) zoomed view of upper band Sdd21.

Figure 2 shows that lowering temperature results in higher resonant frequency for each band. On the contrary, for  $\beta_1 = -30$  ppm/°C, it is seen that as the temperature decreases, the resonant frequency also goes down (Figure 3). Referring to Table 3, for positive value of  $\beta_1$ , the deviation in center frequency is higher than that for negative value of  $\beta_1$ , but the deviation in ABW is almost the same for both cases.

### 2.3. Comparison with Single-Ended Design

In a single-ended design, the vias to the ground add more parasitic resistance to the design, and as a result, the design suffers from more return loss and insertion loss than its differential counterpart. A via acts as an inductor, and its inductance is calculated using Equation (5). Moreover, in the two-port

**Table 3.** Deviations of center frequency and absolute bandwidth of the filter response with temperature variation.

$\beta_1$	Temperature variation range	Deviation in center frequency ( $\Delta f_1, \Delta f_2$ )	Deviation in ABW ( $\Delta ABW_1, \Delta ABW_2$ )
+30 ppm/°C	(−50°C)–125°C	0.43%, 0.37%	0.01%, 0%
−30 ppm/°C	(−50°C)–125°C	0.17%, 0.15%	0.02%, 0.02%

design,  $L_{P1}$  &  $L_{P2}$  values become half, and capacitors  $C_{P1}$  &  $C_{P2}$  values become twice of those values in the differential design. As can be seen from the datasheets, the 0402 series wirewound inductors from Johanson Technology demonstrate lower Q-value for lower inductor value whereas the 0805 series capacitors from the same manufacturer exhibit lower Q value for higher capacitance values. Therefore, as a combined effect, the loss associated with the single-ended filter is higher than its differential counterpart at any temperature. The single-ended counterpart of the differential design (Figure 1(a)) is shown in Figure 4.

$$L_{via} = 5.08h \left[ \ln \left( \frac{4h}{d} + 1 \right) \right] \text{ nH} \quad (5)$$

where  $d$  = via barrel length in inches and  $h$  = thickness of the PCB in inches.

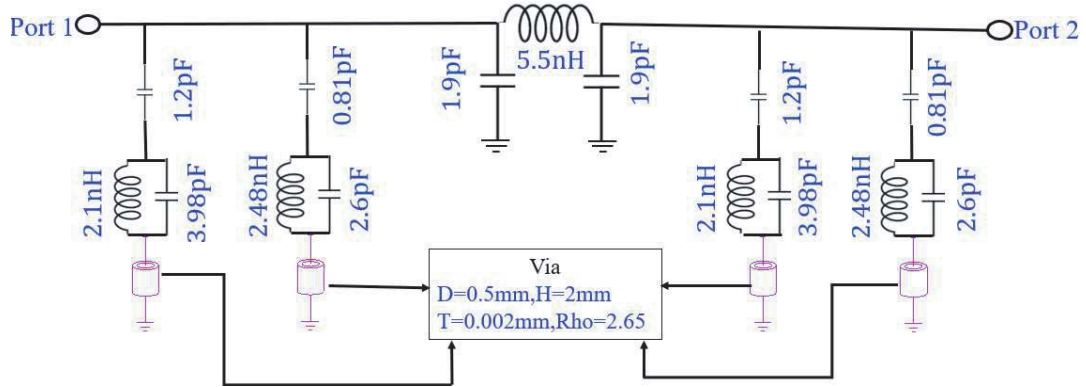


**Figure 4.** Single-ended dual-band BSF where Aluminum ( $Rho = 2.65$ ) vias of diameter ( $D$ ) = 0.5 mm, length ( $H$ ) = 2 mm and thickness ( $T$ ) = 0.002 mm are used.

Considering all real components as well as the via effect, Figure 5 and Figure 6 demonstrate the simulation results for  $\beta_1 = -30$  ppm/°C and  $\beta_1 = +30$  ppm/°C, respectively. Figure 5 shows that at room temperature, the two stopbands are centered at 1.156 GHz and 1.357 GHz, respectively. As the temperature is increased from −50°C to 125°C, the maximum shift observed for any stopband center frequency is about 2 MHz. Similarly, the deviations in the ABWs of the lower and upper bands are also found to be about 2 MHz. Also, the lower band shows a 1.5 dB deviation in insertion loss whereas this change for the upper band is 1 dB. With  $\beta_1 = +30$  ppm/°C, the deviations noticed for the center frequency and the ABW values of the lower band are 5 MHz and 1.8 MHz, respectively (Figure 6). The same parameters for the upper band are shifted by 5 MHz and 1.6 MHz, respectively. The variations in the insertion loss values at resonance are 1.52 dB and 1 dB for the lower band and upper band, respectively.

Based on the frequency response under changing temperature, the single-ended and the differential BSFs are compared in Table 4. For the positive value of  $\beta_1$ , both the differential and single-ended designs exhibit more deviations in terms of center frequency than the deviations for negative  $\beta_1$  value. However, comparing all four cases in terms of ABW, the single-ended design shows at least 0.13% more deviation than the differential design. Also, as expected earlier, the insertion loss at resonance for both bands of the 2-port design is at least 3 dB greater than the 4-port design. Moreover, for the same range

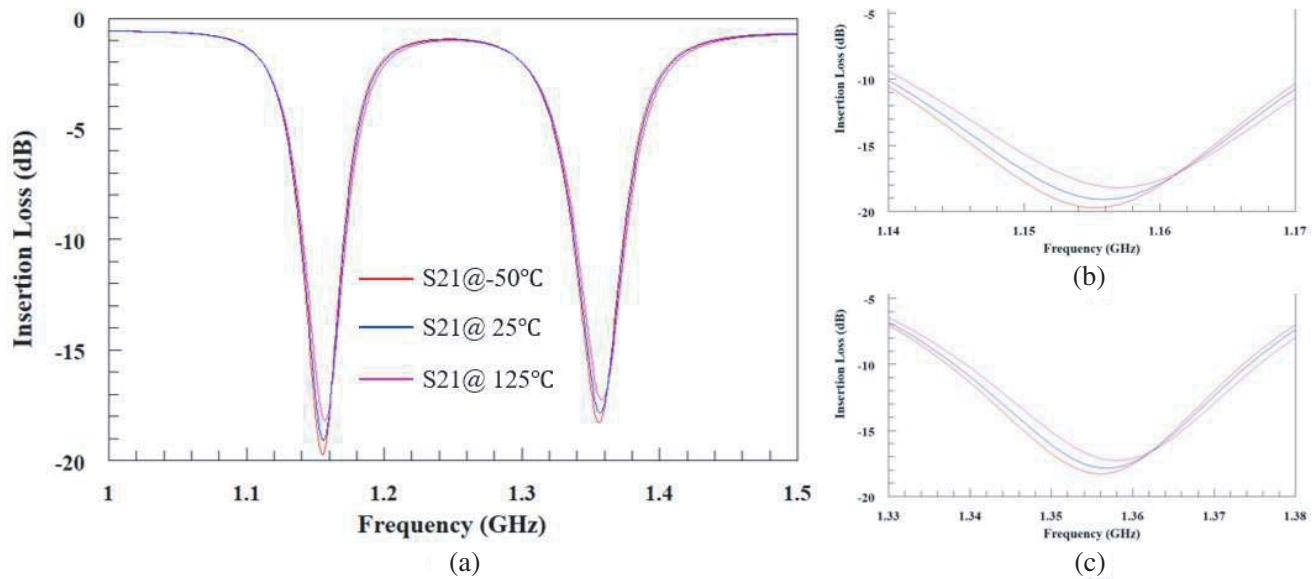


**Figure 5.** Temperature effect on a single-ended design ( $\beta_1 = -30 \text{ ppm}/^\circ\text{C}$ ). (a) Insertion loss (S21) vs. frequency, (b) zoomed view of the lower band S21, (c) zoomed view of the upper band S21.

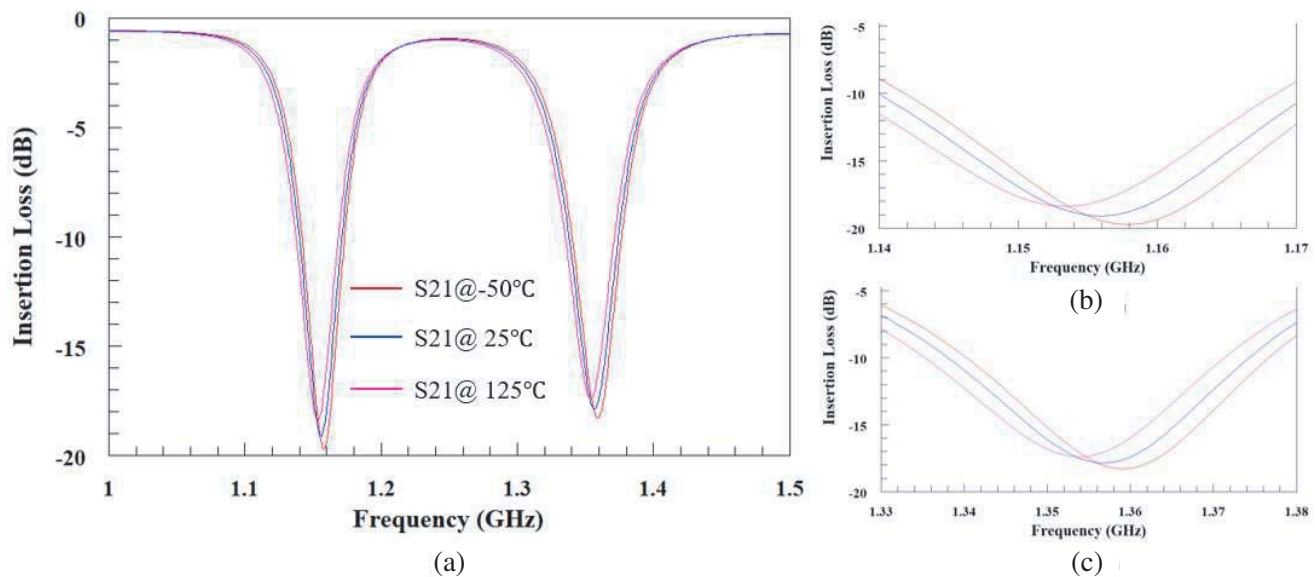


**Figure 6.** Temperature effect on a single-ended design ( $\beta_1 = +30 \text{ ppm}/^\circ\text{C}$ ). (a) Insertion loss (S21) vs. frequency, (b) zoomed view of the lower band S21, (c) zoomed view of the upper band S21.

of temperature variation, the single-ended design shows more discrepancy in the Sdd21 value than the differential structure.

### 3. RESULTS AND DISCUSSIONS

Figure 7(a) shows the fabricated prototype of the filter which is used as the device under test (DUT) here. Figure 7(b) shows the lab setup where the DUT is placed on a holder above the hot plate. One thermocouple is mounted on the filter, and the generated temperature dependent voltage is measured with an Extech Mini multimeter which is calibrated in temperature. The temperature readings here are

**Table 4.** Comparison of the single-ended and the differential BSF designs for the  $((-50^{\circ}\text{C})-(+125^{\circ}\text{C}))$  temperature range.

$\beta_1$	Filter Type	$\Delta f_1, \Delta f_2$	$\Delta ABW_1, \Delta ABW_2$	Sdd21 at resonance (@25°C)	$\Delta Sdd21$ with temperature (dB)
+30 ppm/°C	Differential (Figure 2)	0.43%, 0.37%	0.01%, 0%	22 dB, 24 dB	0.11, 0.15
+30 ppm/°C	Single-ended (Figure 6)	0.43%, 0.44%	0.16%, 0.12%	19 dB, 18 dB	1.52, 1
-30 ppm/°C	Differential (Figure 3)	0.17%, 0.15%	0.02%, 0.02%	22 dB, 24 dB	0.11, 0.15
-30 ppm/°C	Single-ended (Figure 5)	0.17%, 0.15%	0.16%, 0.15%	19 dB, 18 dB	1.5, 1

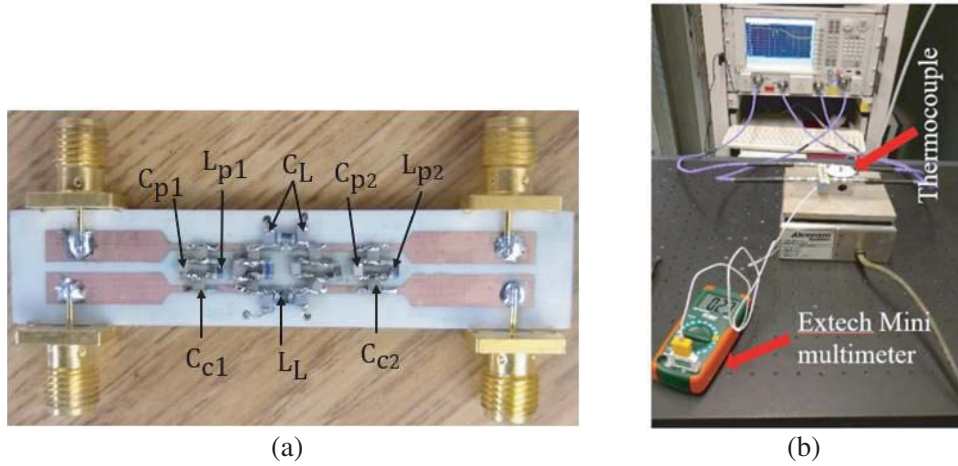


**Figure 7.** (a) Fabricated prototype of the dual-band differential BSF [13] and (b) lab set-up to measure temperature effect on it.

directly taken from the thermocouple as it measures the temperature accurately on the filter. Figure 8 demonstrates that when the temperature is increased from 20°C to 100°C, the lower band frequency changes from 1.151 GHz to 1.148 GHz whereas the upper band frequency varies from 1.366 GHz to 1.361 GHz. As the increased temperature causes the resonant frequency to go down, it is confirmed that the  $\beta_1$  value is a positive number. Also, the shift in center frequency for each band is slightly higher than the simulation result. This comes from the effect of external factors such as thermal expansion/contraction of the cables (the portion above the hot plate) and the connectors due to the continuous change in operating temperature. Due to the unavailability of a temperature forcing system such as Thermonics in the lab, it was not possible to test the filter performance at a temperature lower than 20°C. However, both experimental and simulated results discussed here demonstrate that the deviation per 20°C is almost linear. Therefore, if we extrapolate these results to  $-50^{\circ}\text{C}$ , the maximum deviations for lower band and upper band center frequencies are expected to be about 4 MHz and 9 MHz, respectively. For the experimental 20°C–100°C temperature range, the ABW variation ranges of the lower band and upper band are calculated as 72.1 MHz–73.4 MHz and 77.9 MHz–80.7 MHz, respectively. Moreover, the Sdd21 values for the lower band and upper band resonant frequencies vary by 0.6 dB and 2 dB, respectively. On the other hand, the Sdd11 values of the lower band and upper band resonant frequencies vary by 0.3 dB and 0.2 dB, respectively.

Table 5 compares this work to the related work in literature. From the second column of the table,

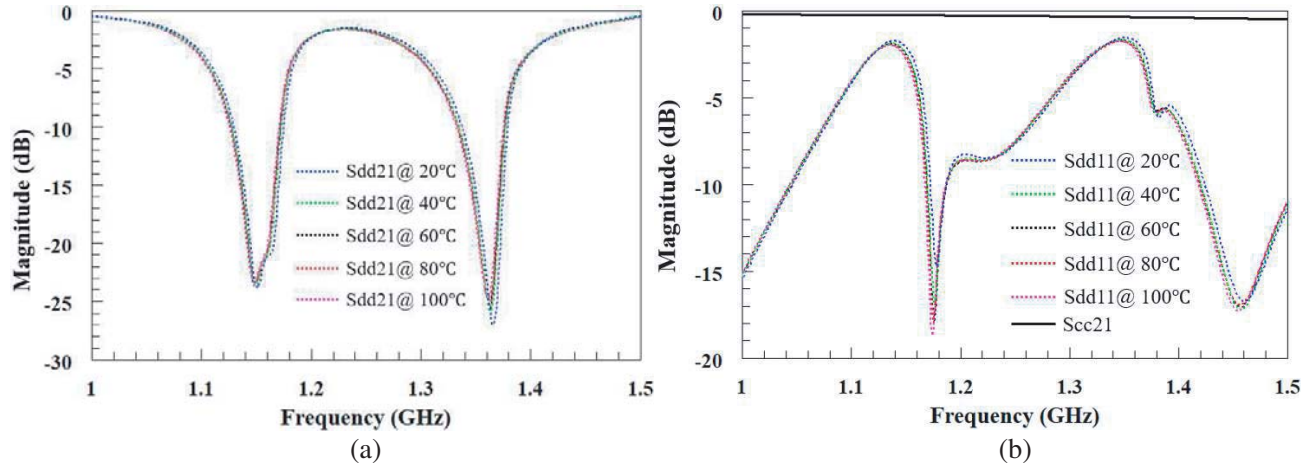


**Figure 8.** Characterization of the dual-band differential filter prototype with temperature variation. (a) Sdd21 (differential insertion loss) and (b) Sdd11 (differential return loss) and Scc21 (common mode insertion loss).

this temperature effect on a differential filter has been examined here for the first time. Moreover, it is a dual-band filter response whereas all other designs incorporate with only one frequency band (third column). From the fourth column, the filter response is tested for a much higher temperature variation range (80°C) than [16–18] (35°C–40°C). For this wide temperature range, the proposed filter shows only 0.2–0.3% shift in center frequency whereas other designs (except [20]) demonstrate at least 0.6% variation for a temperature sweep of only 35°C (fifth column). Although [20] exhibits only 0.02% shift in center frequency, it shows the maximum fluctuation in the stopband rejection level (15 dB) among all the designs (sixth column). Compared to this, the engineered design is very stable which shows a maximum shift of only 2 dB for a 0.2% shift in resonant frequency. Also, as mentioned before, even if this engineered differential design is examined for a temperature range of  $-50^{\circ}\text{C}$  to  $125^{\circ}\text{C}$ , this deviation of its center frequency will not exceed 0.35% (or 4 MHz) and 0.6% (or 9 MHz) for the lower band and upper band, respectively. This means that for this wider temperature range also, this design will offer better performance than most of the designs listed here. For further improvement of its functionality, a similar temperature compensation circuit presented in [14] can be considered.

**Table 5.** Comparison of state-of-art BSF structures to the proposed design in terms of performance under different thermal conditions.

Ref.	Filter Type	# of frequency bands	$\Delta\text{Temp. range}$	%shift @center frequency (GHz)	$\Delta\text{Sdd21 range}$ (dB)
[16]*	Single-ended	1	35°C (25°C–60°C)	(a) $\sim 2\%$ @7.2 (b) $\sim 2\%$ @26 (c) $< 2\%$ @35.2	(a) 1.2 (4.8 to 6) (b) 1.2 (5 to 6.2) (c) 1.5 (8.5 to 10)
[17]	Single-ended	1	39°C (25°C–64°C)	$\sim 0.58\%$ @10.36	1 (35 to 36)
[18]	Single-ended	1	35°C (24°C–59°C)	$\sim 0.9\%$ @2.4	- - -
[19]	Single-ended	1	100°C ((-30)°C–70°C)	5.6%@5.8	2 (28 to 30)
[20]	Single-ended	1	100°C ((-25)°C–75°C)	0.02%@24.665	15 (30 to 45)
<b>This work</b>	<b>Differential</b>	<b>2</b>	<b>80°C</b> (20°C–100°C)	<b>0.2%@1.151,</b> <b>0.3%@1.366</b>	<b>0.6 (23.2 to 23.8)</b> <b>2 (25 to 27)</b>

\* Three filter architectures.

#### 4. CONCLUSION

In this paper, an investigation is conducted to see how the operating temperature affects the functionality of a lumped element differential dual-band band-stop filter (BSF). First, the temperature effect on ideal inductor and capacitor is discussed qualitatively, and then simulation is performed considering parasitic resistance associated with the real components. These simulation results are compared to those from its equivalent single-ended BSF to show better performance in terms of both loss and ABW deviation. Finally, for practical validation, a fabricated dual band differential BSF prototype operating at 1.15 GHz and 1.37 GHz is tested for a temperature range of 20°C–100°C. The experimental results are compared to the simulation ones to show a good match between them. Compared to the state-of-the-art designs, this engineered design proves to be more robust with temperature change. The design shows only 0.2 to 0.3% shift in resonant frequencies for a variation of 80°C from the room temperature while the maximum deviation found in terms of stopband rejection level is only 2 dB. This makes the proposed filter useful for any industrial, military, and automotive applications.

#### REFERENCES

1. Borah, D., “Differential multiband reconfigurable filters for RF front-end applications,” Ph.D. Dissertation, May 2020.
2. Chiou, Y.-C. and J.-T. Kuo, “Planar multiband bandpass filter with multimode stepped-impedance resonators,” *Progress In Electromagnetics Research*, Vol. 114, 129–144, 2011.
3. Li, X. and H. Wang, “An approach for multi-band bandpass filter design based on asymmetric half-wavelength resonators,” *Progress In Electromagnetics Research*, Vol. 140, 31–42, 2013.
4. Borah, D. and T. S. Kalkur, “A balanced dual-band tunable bandpass filter,” *2018 International Applied Computational Electromagnetics Society Symposium (ACES)*, 1–2, Denver, CO, 2018.
5. Wang, J., H. Ning, Q. Xiong, M. Li, and L.-F. Mao, “A novel miniaturized dual-band bandstop filter using dual-plane defected structures,” *Progress In Electromagnetics Research*, Vol. 134, 397–417, 2013.
6. Hagag, M. F., M. Abdelfattah and D. Peroulis, “Balanced octave-tunable absorptive Band-stop filter,” *2018 IEEE 19th Wireless and Microwave Technology Conference (WAMICON)*, 1–4, Sand Key, FL, 2018.
7. Sorocki, J., I. Piekarczyk, S. Gruszczynski and K. Wincza, “Low-loss directional filters based on differential band-reject filters with improved isolation using phase inverter,” *IEEE Microwave and Wireless Components Letters*, Vol. 28, No. 4, 314–316, Apr. 2018.
8. Kong, M., Y. Wu, Z. Zhuang, and Y. Liu, “Narrowband balanced absorptive Band-stop filter integrated with wideband bandpass response,” *Electronics Letters*, Vol. 54, No. 4, 225–227, Feb. 22, 2018.
9. Cai, J., Y. Yang, W. Qin, and J. Chen, “Wideband tunable differential band-stop filter based on double-sided parallel-strip line,” *IEEE Transactions on Components, Packaging and Manufacturing Technology*, Vol. 8, No. 10, 1815–1822, Oct. 2018.
10. Borah, D. and T. S. Kalkur, “A planar multiband balanced bandstop filter,” *2018 IEEE MTT-S Latin America Microwave Conference (LAMC 2018)*, 1–3, Arequipa, Peru, 2018.
11. Borah, D. and T. S. Kalkur, “Tunable multiband balanced bandstop filter with high CMRR,” *Progress In Electromagnetics Research C*, Vol. 97, 1–13, 2019.
12. Borah, D. and T. S. Kalkur, “Ultra-compact balanced multiband fully reconfigurable bandstop filter,” *Progress In Electromagnetics Research C*, Vol. 100, 133–143, 2020.
13. Borah, D. and T. Kalkur, “Lumped element balanced multi-band bandstop filter for ultra high frequency applications,” *The Journal of Engineering*, 1–5, 2020.
14. Abu Khater, M., K. Zeng, and D. Peroulis, “Temperature-compensated lumped element tunable bandpass filter,” *2016 IEEE MTT-S International Microwave Symposium (IMS)*, 1–4, San Francisco, CA, 2016.

15. De la Torre Rodríguez, L. M., et al., "Predicting the effect of variations in ambient temperature and operating power on the response of a microwave filter," *2016 Loughborough Antennas & Propagation Conference (LAPC)*, Loughborough, 2016, 1-5.
16. Muller, A., R. A. Khadar, T. Abel, N. Negm, T. Rosca, A. Krammer, M. Cavalieri, A. Schueler, F. Qaderi, J. Bolten, M. Lemme, I. Stolichnov, and A. M. Ionescu, "Radio-frequency characteristics of Ge-doped vanadium dioxide thin films with increased transition temperature," *ACS Applied Electronic Materials*, Vol. 2, No. 5, 1263–1272, 2020.
17. Katzin, P., B. Bedard, and Y. Ayasli, "Narrow-band MMIC filters with automatic tuning and Q-factor control," *IEEE 1993 Microwave and Millimeter-Wave Monolithic Circuits Symposium Digest of Papers*, 141–144, Atlanta, GA, USA, 1993.
18. Su, W., C. Mariotti, B. S. Cook, S. Lim, L. Roselli, and M. M. Tentzeris, "A metamaterial-inspired temperature stable inkjet-printed microfluidic-tunable bandstop filter," *2014 44th European Microwave Conference*, 9–12, Rome, 2014.
19. Wu, Z., Y. Shim, and M. Rais-Zadeh, "Miniaturized UWB filters integrated with tunable notch filters using a silicon-based integrated passive device technology," *IEEE Transactions on Microwave Theory and Techniques*, Vol. 60, No. 3, 518–527, Mar. 2012.
20. Schallner, M., "Temperature compensated planar narrow-band notch filter with fully automated laser-trimming," *2001 IEEE MTT-S International Microwave Symposium Digest (Cat. No.01CH37157)*, Vol. 3, 1919–1922, Phoenix, AZ, 2001.